Available online at www.sciencedirect.com
SCIENCE DIRECT®
Journal of Nuclear Materials 341 (2005) 164–168
journal of nuclear materials
www.elsevier.com/locate/jnucmat

Microstructure and non-equilibrium phases in electron beam-welded joints of Al–Fe–Ce and Zircaloy-4

M. Ahmad [a], J.I. Akhter [a,*], M. Iqbal [a], M. Akhtar [a], E. Ahmed [a], S. Akhtar [b], M.A. Chaudhary [c]

[a] *Physics Research Division, Pakistan Institute of Nuclear Science and Technology, P.O. Nilore, Islamabad, Pakistan*
[b] *Nucleonic Systems Labs., PINSTECH, P.O. Nilore, Islamabad, Pakistan*
[c] *Physics Department, Islamia University Bahawalpur, Pakistan*

Received 5 October 2004; accepted 17 January 2005

Abstract

Electron beam welding (EBW) of Zircaloy-4 and Al–Fe–Ce alloys is carried out to investigate the microstructure and non-equilibrium phases produced in the molten zone (MZ). Scanning electron microscopy (SEM) with an energy dispersive system (EDS) attachment and X-ray diffraction (XRD) are used to characterize the microstructural and compositional changes and phases. Five distinct regions containing various phases are observed in the MZ. Hot cracking is observed in the region containing $AlZr_2$ and Al_2Zr_3 intermetallic compounds.

1. Introduction

From the practical point of view, it may not be possible to join materials by fusion if the melting temperatures of two alloys differ a lot, as it is necessary to have controlled melting on both sides of the simultaneous weld joints. Even if this criterion is met, it may not be possible to have an appropriate joint, if the two materials are metallurgically incompatible. This is because metallurgical incompatibility may lead to a weld zone and heat-affected zones (HAZs) of which the microstructure could not provide adequate mechanical properties. Cracking during welding can be a problem in Al-base alloys. This occurs due to relatively high thermal expansion, large change in volume upon solidification and wide solidification temperature range. Weld solidification cracks can be eliminated or be controlled with the addition of filler metal [1,2]. However, the additives may modify the base material constituents and may not always be desirable.

A high energy beam process such as EBW is a fusion joining of materials under higher level of vacuum to avoid the oxidation of joints. The main advantage is that it results in localized melting, minimal heat input and high cooling rate. The welds produced by this technique have reduced HAZs and cracks in welds of Al-base alloys [3–6] and minimized the brittle phase in the joints of Zircaloy-4 and stainless steel [7]. Laser welding can also be employed under similar considerations. However, due to low penetration of the laser beam compared

* Corresponding author. Tel.: +92 51 2207224; fax: +92 51 9290275.
E-mail address: akhterji@pinstech.org.pk (J.I. Akhter).

0022-3115/$ - see front matter © 2005 Elsevier B.V. All rights reserved.
doi:10.1016/j.jnucmat.2005.01.020

to electron beam and strong reflection of laser beam from Al, laser welding of Al alloys is less effective [8,9].

Aluminum and zirconium alloys are used in nuclear industry as internal materials and have drastic differences in their melting points and thermal expansion coefficients and it is very difficult to join them with any welding technique. There is no report available on the welding of such incompatible materials. The main aim of the present work is to investigate the microstructure and non-equilibrium phases formed in the molten zone (MZ) of the welded joints of dissimilar materials such as Al–Fe–Ce and Zircaloy-4 having high incompatibility.

2. Experimental

Samples of size $10 \times 20 \times 2$ mm^3 were cut from the alloys having compositions given in Table 1. Joining surfaces were polished with diamond paste on the lapping machine down to 0.25 μm and placed side by side in a die made of copper to have good contact during welding. The parameters used for welding are, voltage =40 kV, current = 20 mA, weld travel speed = 600 mm/min with the beam in vibration mode. In order to reveal the microstructure, the samples were etched in a solution of 50 ml H_2O_2, 47 ml HNO_3 and 3 ml HF. Microstructural investigations were done using scanning electron microscopy (SEM) and the analysis of phases was carried out with an energy dispersive system (EDS). Phases were also identified with the X-ray diffraction (XRD) technique.

3. Results and discussion

The low-magnification view of the EBW sample, taken by the backscattered detector is shown in Fig. 1. It reveals five distinct regions namely I, II, III, IV and V in the MZ. The region I at higher magnification is shown in Fig. 2 and gives white contrast in the secondary electron emission image (SEI). EDS analysis indicates that it is enriched in Zr, Sn and Al. The layer is very smooth and shows black contrast in the backscattered image (BEI) in Fig. 1, which also indicates the presence of higher Sn content in this region. The average composition of this region is given in Table 2 and shows that this layer is β-Zr and it resists the diffusion of Al, Fe and Ce towards Zircaloy-4. The region II in the MZ having Widmanstätten structure in the beginning and solidification cracking towards the region III is shown in Fig. 3. Microcracks are also observed in this region. The composition of the region is also given in Table 2, which indicates that the region consists of the $AlZr_2$ intermetallic compound along with α-Zr plates. The density of the cracks decreases in the beam travel direction. The region III in the MZ consists of an intermetallic compound rich in Zr and Al and gives white contrast in the

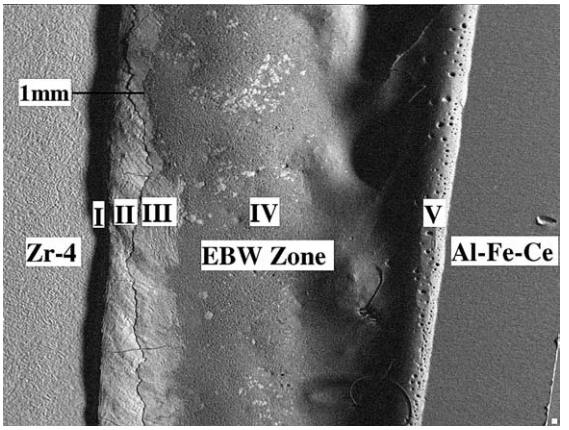

Fig. 1. BEI micrograph (backscattered electron image) clearly indicating different regions in the EBW zone.

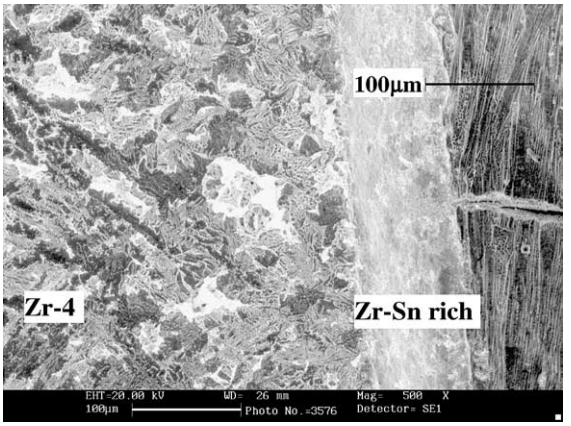

Fig. 2. SEI micrograph (secondary electron image) showing the Zr–Sn rich region giving white contrast in the image.

Table 1
Composition of Zircaloy-4 and the Al–Fe–Ce alloy in wt%

Alloy/element	Al	C	Ce	Cr	Fe	Ni	Sn	Zr
Zircaloy-4	–	0.002	–	0.10	0.20	< 0.005	1.52	Balance
Al–Fe–Ce	92.71	–	2.53	–	4.76	–	–	–

Table 2
Quantitative X-ray analysis of different layers/precipitates formed in EBMZ

Regions	Elements	Concentration (in wt%)	Phases	Shapes
I	Al	4.89	β-Zr	Layer
	Fe	1.77		
	Zr	81.90		
	Sn	11.45		
II	Al	11.89	$AlZr_2$	Layer
	Fe	1.07		
	Zr	87.03		
III	Al	15.41	Al_2Zr_3	Plates
	Fe	–		
	Zr	84.59		
Beginning of IV	Al	37.34	Al_2Zr	Rectangular type
	Fe	0.87		
	Zr	60.89		
	Ce	0.90		
IV	Al	41.09	Al_3Zr	Rod
	Zr	58.26		
	Fe	0.65		
IV near V	Al	55.29	Al_3Fe	Rod
	Fe	31.58		
	Zr	10.13		
	Sn	3.00		
V	Al	85.31	Eutectic	
	Fe	3.60		
	Zr	9.00		
	Sn	0.35		
	Ce	1.75		

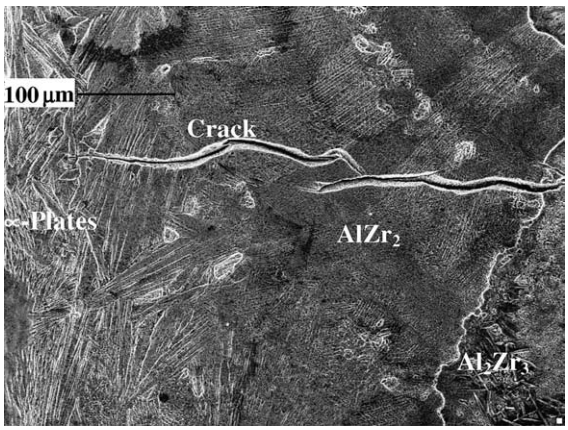

Fig. 3. SEI micrograph showing hot cracking in the MZ near Zircaloy-4 having the composition of $AlZr_2$.

backscattered electron image shown in Fig. 4. EDS analysis of this intermetallic compound indicates that the

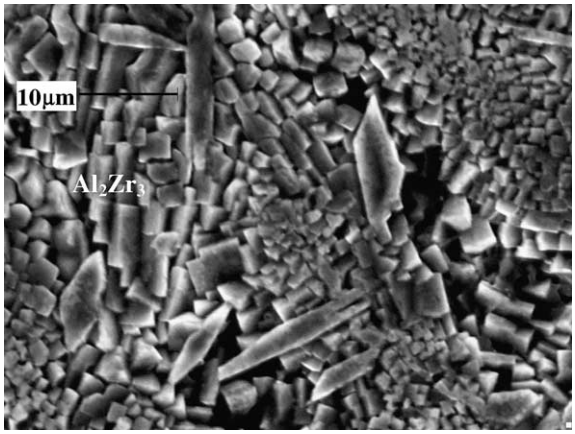

Fig. 4. BEI micrograph of Al_2Zr_3 phase in the beginning of EBW region, III.

composition corresponds to Al_2Zr_3. It is also observed that the area of the regions II and III having $AlZr_2$ and Al_2Zr_3 intermetallic compounds reduces as the welding proceeds. This is likely due to the fast diffusion of Al towards Zircaloy-4 in the MZ as the Al–Fe–Ce alloy has a low melting temperature and Al has a higher diffusion coefficient compared to Zr.

Generally the solidification cracking of a weld pool alloy depends on the combination of mechanically and thermally induced strain and a crack-susceptible microstructure of the solidified weld zone. It is also considered that solidification cracking of weld pool alloy is dependent on the liquid-to-solid freezing temperature range [3], which is defined as the difference between the liquidus and the solidus temperature during the solidification process. The wider solidification temperature range of the alloy has more sensitivity towards the solidification cracking. The equilibrium phase diagram [10] indicates that the range of freezing temperature is very large. So the large freezing temperature range of the system under study may be a possible cause of solidification cracking. The formation of $AlZr_2$ and Al_2Zr_3 intermetallic compounds generates the regions of cracking due to their brittle nature and difference in shrinkage as compared to the other regions. A dendritic or eutectic structure is not observed in these regions, which might be due to the slow cooling on the Zircaloy-4 side as compared to Al–Fe–Ce alloy because the thermal conductivity of Zr is 11 times less compared to Al. The thermal expansion coefficients of Al-alloys are about four times higher than those of Zircaloy-4 and the shrinkage is also larger in the Al-alloys compared to Zircaloy-4 during cooling. So the thermal stress and shrinkage would be higher in the weld zone near the Al–Fe–Ce alloy compared with the weld zone near the Zircaloy-4, whereas the cracking is observed in the MZ near Zircaloy-4 only. Region IV contains Al_3Zr rod type and Al_2Zr rectangular type

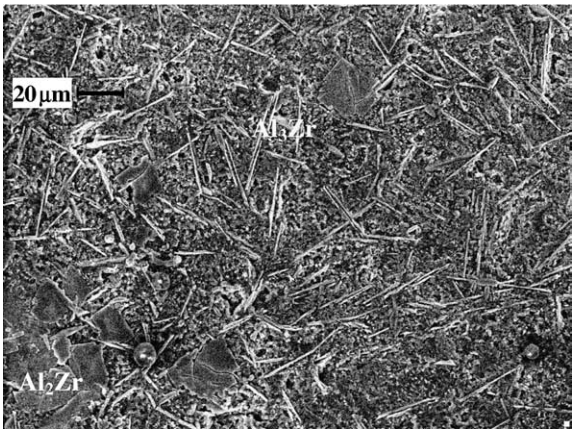

Fig. 5. SEI micrograph showing the Al_2Zr phase (rectangular shape with gray contrast) in the molten zone IV along with rod type Al_3Zr precipitates.

precipitates as shown in Fig. 5 and the composition is given in Table 2. This phase is observed only in the beginning of region IV and the density of this phase is very low compared to Al_3Zr. As the rectangular shape Al_2Zr disappears the density of Al_3Zr increases. It is also observed that the concentration of Fe increases in the rod type precipitates near the region V and the precipitates are found by EDS to be Al_3Fe. The matrix structure in this region is eutectic which is known to be resistant against solidification cracking [7].

Droplets of circular shape, rich in Al and containing minute quantities of Zr, are found in region V. These droplets solidify as liquids and are shown in Fig. 6. The matrix in region V is also of eutectic nature with the structure being finer compared to that in region IV. Fine eutectic structures and droplets of pure Al are formed due to deep undercooling occurring in this area because of the higher thermal conductivity of the Al–Fe–Ce alloy. Fig. 1 also shows cavities/voids/pores in the MZ adjacent to the solid Al–Fe–Ce alloy in region V. The formation of these cavities as well as the eutectic structure indicate that the maximum supercooling occurred at the side of the Al–Fe–Ce alloy. Due to the higher level of supercooling, a higher fraction of the solidification process occurs near zero hydrostatic pressure, i.e. the condition is favorable for the formation of the cavities [11]. So the existence of both the fine eutectic structure and the cavities confirms that the higher supercooling has been obtained in the region near to the solid Al–Fe–Ce alloy.

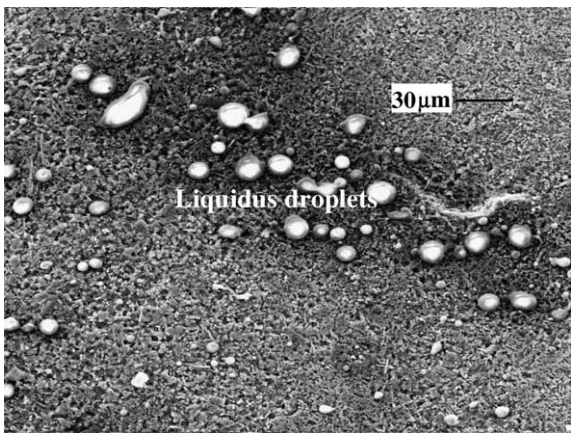

Fig. 6. SEM micrograph showing liquidus droplets with white contrast in region V of the MZ.

Table 3
Analysis of phases in EBW zone characterized by XRD technique

Identified phases	*d*-Spacing	(*hkl*)
Al_2Zr_3	5.40	(110)
Al_3Zr	4.371	(004)
$AlZr_2$	3.47	(101)
Al_3Zr	3.318	(103)
Al_3Zr, α-Zr	2.799	(110), (100)
α-Zr, Al_2Zr_3	2.576	(002), (202)
Al_2Zr_3, α-Zr	2.456	(212), (101)
Al_2Zr_3	2.427	(310)
Al_3Zr	2.36	(114)
Al	2.328	(111)
Al_2Zr_3, Al_3Zr	2.152	(113), (008)
Al_2Zr_3	2.097	(320)
Al, Al_3Zr, Al_2Zr_3	2.017	(200), (200), (321)
Al_2Zr_3	1.849	(410)
Al_3Zr, Al_2Zr_3	1.738	(109), (004)
Al_2Zr_3	1.691	(420)
α-Zr, Al_3Zr, Al_2Zr_3	1.598	(110), (215), (332)
Al_2Zr_3	1.553, 1.502	(214), (510)
α-Zr, Al_3Zr	1.463	(103), (208)
Al_2Zr_3, Al_3Zr, Al	1.426	(333), (220), (220)
Al_2Zr_3, α-Zr	1.384	(521), (200)
Al_3Zr, α-Zr	1.338, 1.296	(301), (11,12), (201), (004)
Al_3Zr	1.25	(10,13)
Al, Al_3Zr, α-Zr	1.217	(311), (314), (202)
Al_3Zr	1.191	(228)
Al, α-Zr	1.168	(222), (104)

X-ray diffraction analysis of the EBW sample is given in Table 3. The phases identified are $AlZr_2$, Al_2Zr_3, Al_3Zr along with Zr and Al–Fe–Ce. The remaining phases detected by SEM/EDS are not found by X-ray diffraction. The reason may be that the volume density of the Al_2Zr and Al_3Fe phases is very low compared to the matrix in the bulk sample and may be beyond the detection limit of our XRD instrument. EDS is a more powerful technique for point-to-point analysis and can detect the phases present in the localized areas.

4. Conclusions

The phases produced in the weld zone of Zircaloy-4 and Al–Fe–Ce alloys have been clearly characterized. Cracking in the regions II and III occurs due to the intermetallic compounds $AlZr_2$ and Al_2Zr_3. The β-Zr phase rich in Sn and Al forms near Zircaloy-4 in the form of layers which might act as barrier against the diffusion of Al, Fe, Ce towards the Zircaloy-4. The area of the intermetallic compounds $AlZr_2$ and Al_2Zr_3 is found to reduce in the weld travel direction while the area of region IV having rod type precipitates and region V having voids with the eutectic matrix structure increases towards the weld direction.

Acknowledgment

The authors are very thankful to the staff members of the Radiation Damage Group of Physics Research Division for their assistance throughout the experimental phase of this research work.

References

[1] J.H. Dudas, F.R. Collins, Welding J. 45 (1966) 241-s.
[2] M. Katoh, H.W. Kerr, Proceedings of the International Conference on Trends in Welding Research, ASM International, Metals Park, OH, 1986, 759.
[3] H.T. Kim, S.W. Nam, S.H. Hwang, J. Mater. Sci. 31 (1996) 2859.
[4] S. Tosto, F. Nenci, J. Hu, Mater. Sci. Technol. 12 (1996) 323.
[5] F. Matsuda, K. Nakata, Trans. JWRI 11 (1982) 141.
[6] J.R. Davis (Ed.), ASM Specialty Handbook: Aluminum and Aluminum Alloys, ASM International, Metals Park, OH, 1993.
[7] M. Ahmad, J.I. Akhter, M.A. Shaikh, M. Akhtar, M. Iqbal, M.A. Chaudhry, J. Nucl. Mater. 301 (2002) 118.
[8] B.A. Mehmetli, K. Takahashi, S. Sato, Appl. Opt. 35 (1996) 3237.
[9] L.A. Guitterz, G. Neye, E. Zschech, Welding J. 75 (1996) 115.
[10] M. Alatalo, M. Weinert, R.E. Watson, Phys. Rev. B 57 (1998) R2009.
[11] M.E. Glicksman, Acta. Metall. 13 (1965) 1231.